CHAPTER 15

Nonequilibrium Reactions—Martensitic and Bainitic Structures

WHILE MANY OF THE transformations discussed so far occur under equilibrium or near-equilibrium conditions, martensitic and bainitic structures are produced by nonequilibrium cooling. In both cases, the alloy is heated to a sufficiently high temperature and then suddenly cooled (quenched) to a much lower temperature. Both martensitic and bainitic transformations are extremely important strengthening mechanisms for iron-carbon base-alloys.

In this chapter, the topics covered include martensitic structures in steels, martensitic structures in nonferrous alloys, shape-memory alloys, and bainitic structures in steels.

15.1 Nonequilibrium Cooling—TTT Diagrams

Equilibrium cooling rates might be approximated by a very large piece of steel undergoing very slow furnace cooling. Under normal industrial processing conditions, the cooling rates are almost always much faster, and new phases that are not on the equilibrium phase diagram can appear. When the cooling rate is extremely rapid, such as when quenching steel from temperatures in the austenite phase field (>740 °C, or 1364 °F) into cold water, the iron-carbon phase diagram can no longer be used because quenching is such a radical departure from equilibrium. At rapid cooling rates, it is necessary to use a time-temperature-transformation (TTT) diagram. These diagrams are so named because they depict Transformations as a function of Time and Temperature.

To construct a TTT diagram, very small samples, approximately the size of a dime, are first heated into the single-phase austenite field; this is also

referred to as austenitization. Samples are then withdrawn from the furnace and immediately quenched into salt baths maintained at a given intermediate temperature. The specimen is held in the salt bath for a precise time and then quenched in a water bath maintained at room temperature. This procedure is shown in Fig. 15.1. At each intermediate temperature, the sample is held for a precise period of time, as shown in the example in Fig. 15.2. After quenching, the samples are examined by metallography to determine the microstructure. In the example, note that the amount of pearlite in the microstructure increases as the length of time in the intermediate salt bath increases. After a series of samples has been evaluated at one temperature, other temperatures are evaluated, for example, 700, 600, 500, 400, 300 °C (1200, 1100, 1000, 900, 800 °F) and so on down toward room temperature. Once the data is collected, it is used to plot the extent of transformation

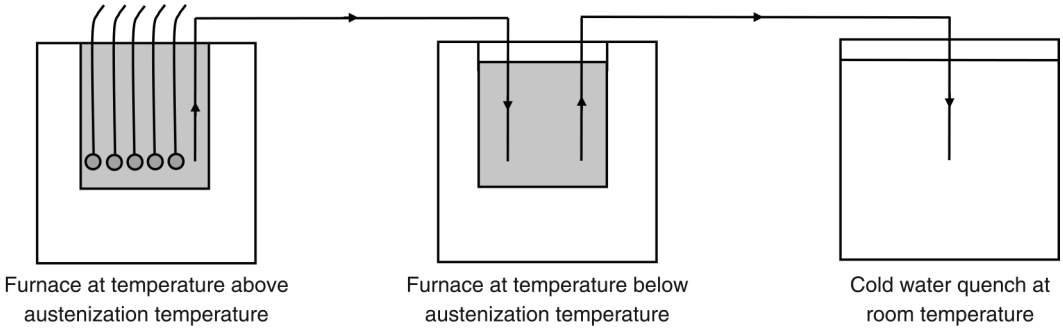

Fig. 15.1 Method for determining isothermal transformations. Source: Ref 15.1 as published in Ref 15.2

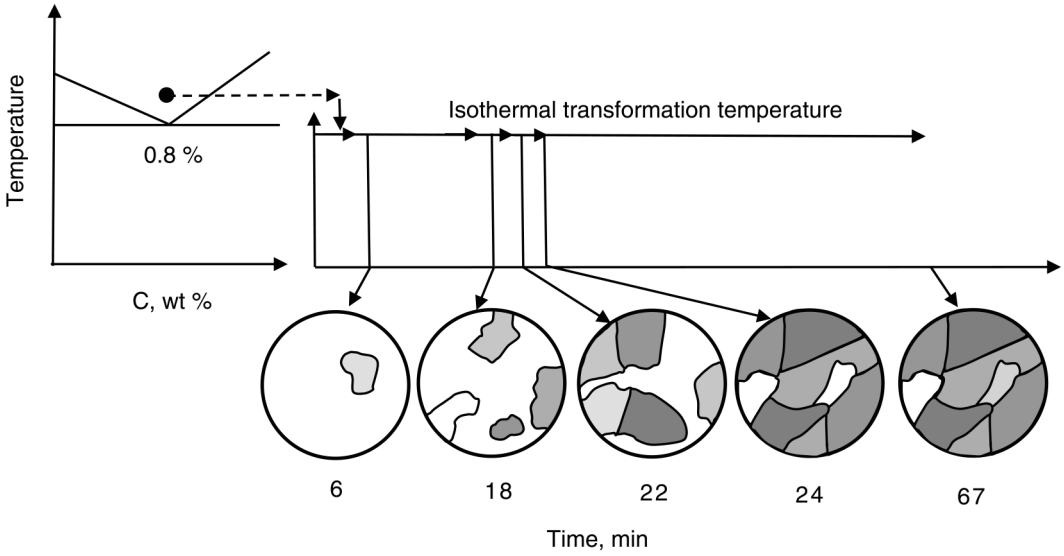

Fig. 15.2 Isothermal transformation of plain carbon steel. Source: Ref 15.1 as published in Ref 15.2

product in the microstructure on a temperature-time plot in the manner shown in Fig. 15.3. A fully developed TTT curve with the transformation products marked on the diagram is shown for the eutectoid plain-carbon steel 1080 in Fig. 15.4, which nominally contains 0.8 wt% C.

A TTT diagram is essentially a visual map that allows one to determine which constituents form as a function of temperature and time. For example, a sample rapidly cooled from the austenitic phase field to a temperature of 600 °C (1110 °F) will begin to transform to pearlite if held at the intermediate temperature for approximately 2 to 3 seconds. On further holding at 600 °C (1110 °F), it will completely transform to pearlite in approximately 10 s. In this particular steel, pearlite forms at all temperatures along the start-of-transformation curve from the A_1 temperature (725 °C, or 1340 °F) to the nose of the diagram (540 °C, or 1000 °F). At the higher transformation temperatures, the pearlite interlamellar spacing is very coarse. The interlamellar spacing is increasingly fine as the temperature decreases toward the nose of the diagram. This is significant because

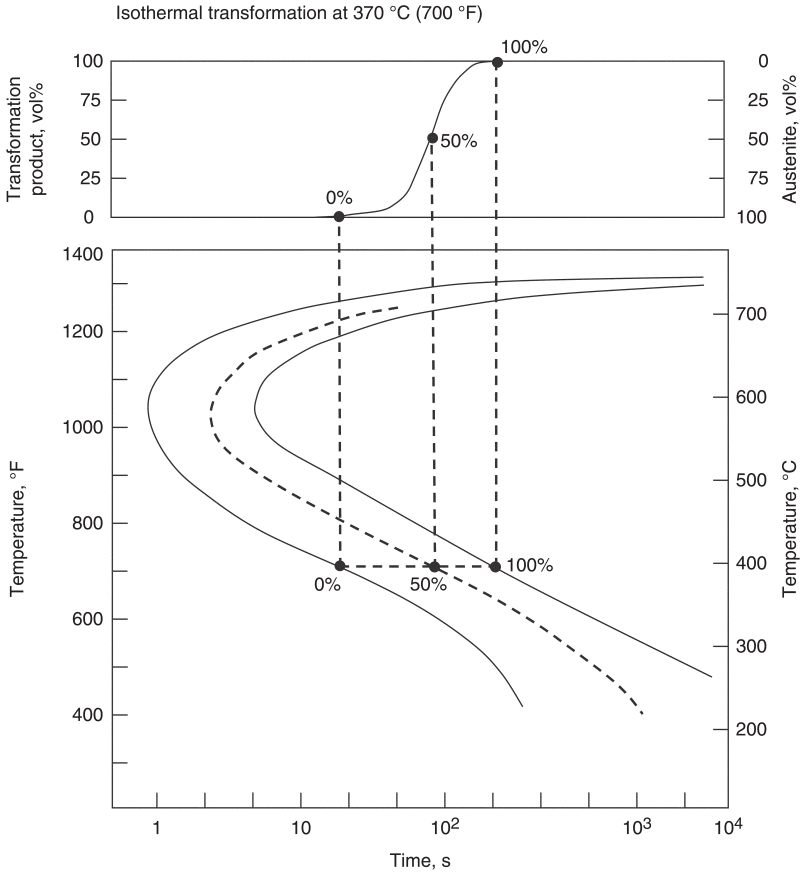

Fig. 15.3 Isothermal transformation curve development. Source: Ref 15.2

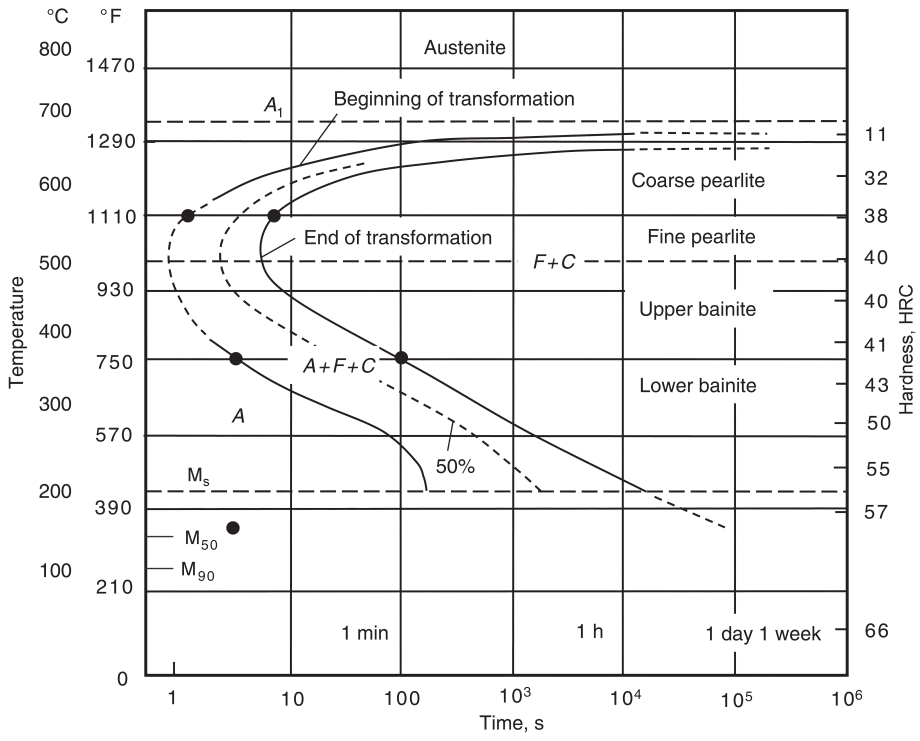

Fig. 15.4 Isothermal transformation diagram for 1080 steel. Source: Ref 15.2

a steel with a coarse pearlite interlamellar spacing is softer and of lower strength than a steel with a fine pearlite interlamellar spacing.

At small amounts of undercooling below the A_1 isotherm, the transformation to pearlite takes a relatively long time to nucleate. As the degree of undercooling increases, the incubation time decreases rapidly, even though the transformation is occurring at lower temperatures where diffusion is less rapid. Eventually, the incubation time reaches a minimum and then begins to increase again. This minimum incubation time occurs at the nose of the TTT diagram. The shape of the TTT diagram is a result of changing reaction kinetics. At high temperatures, the driving force for reaction is lower due to less undercooling, but the diffusion rates are faster, while at lower temperatures, the driving force for reaction is increasing due to greater degrees of undercooling, while the diffusion rates are decreasing due to lower temperatures.

If the steel sample is quenched to 400 °C (750 °F) and held for various times, pearlite does not form; instead, a totally new constituent called bainite forms. Like pearlite, bainite consists of ferrite and cementite, but the morphology is different. Also, note that there are two types of bainite shown on the diagram: upper bainite, which forms at higher temperatures, and lower bainite, which forms at lower temperatures.

Finally, if the specimens are quenched in a salt bath to 150 °C (300 °F), another new constituent, called martensite, forms. Martensite is quite different from both pearlite and bainite. It is not a mixture of ferrite and cementite. Instead, martensite is a form of ferrite that is supersaturated with carbon. Because of the very fast cooling rate, the carbon atoms do not have time to diffuse from their interstitial positions in the body-centered cubic (bcc) lattice to form cementite particles. Because martensite forms suddenly, there are no start-of-transformation or finish-of-transformation curves, as for pearlite and bainite. Instead, there are M_s (martensite start) and M_f (martensite finish) temperatures.

The hardness of the various transformation products is indicated on the right axis of the diagram and shows that the hardness increases with decreasing transformation temperature. Steel products produced with an as-quenched martensitic microstructure are very hard and brittle. Therefore, most martensitic products are tempered by heating to temperatures between approximately 345 and 650 °C (650 and 1200 °F). The tempering process allows some of the carbon to diffuse from the supersaturated iron lattice and form a carbide phase, softening the steel and restoring some ductility. The degree of softening is determined by the tempering temperature and the time at the tempering temperature. The higher the temperature and the longer the time of tempering, the softer the steel becomes. Thus, most steels with martensite are used in the quenched and tempered condition.

Martensitic Structures. As shown previously in the TTT diagram, martensite is a metastable structure that forms during athermal (nonisothermal) conditions. Unlike isothermal decomposition of phase constituents that approach equilibrium conditions by diffusion-controlled mechanisms, martensite does not appear on equilibrium phase diagrams. The mechanism of martensitic transformation is a diffusionless process, where rapid changes in temperature cause shear displacement of atoms and individual atomic movements of less than one interatomic spacing. The transformation also depends on the temperature: martensite begins to form at a M_s temperature, and additional transformation ceases when the material reaches a M_f temperature. The M_s and M_f temperatures depend on the alloying elements in the metal.

In general, martensitic transformation can occur in many types of metallic and nonmetallic crystals, minerals, and compounds, if the cooling or heating rate is sufficiently rapid. The most important example is martensite in steel, when the more densely packed austenite (face-centered cubic, or fcc) phase transforms to the less densely packed crystal structures of either bcc ferrite or body-centered tetragonal (bct) martensite (Fig. 15.5). When steel is slowly cooled from the austenite phase, the crystal structure (size) transforms to the less densely packed ferrite phase. At faster cooling rates, the formation of ferrite is suppressed, while formation of martensite

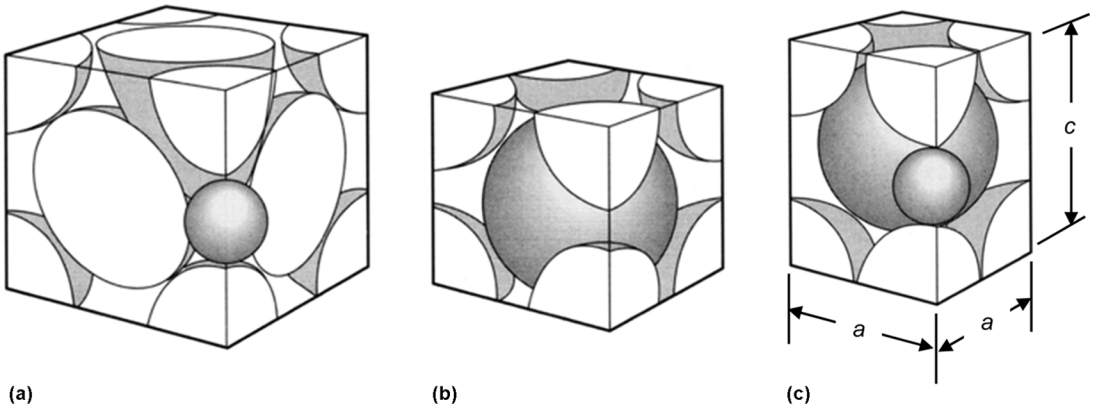

Fig. 15.5 Crystal structures. (a) Austenite (face-centered cubic, fcc). (b) Ferrite (body-centered cubic, bcc). (c) Martensite (body-centered tetragonal, bct). Source: Ref 15.3

is enhanced by the shear displacement of iron atoms into an interstitial, supersaturated solid solution of iron and carbon. This metastable state has bct structure, which is even less densely packed than austenite. This results in lattice distortion that provides strength/hardness by impeding dislocation movements and a volumetric expansion at the M_s temperature. During cooling, when the steel reaches the M_f temperature, the martensitic transformation ceases and any remaining austenite (γ) is referred to as retained austenite.

15.2 Martensite in Steels

Martensite is formed in steels when they are heated into the austenitic field and then rapidly quenched to room temperature. The martensite transformation differs from other phase transformations in several ways: (1) the reaction is a diffusionless phase transformation, (2) no chemical composition change occurs between martensite and the parent phase, (3) there is a coordinated crystal lattice structural change ("military mode") during transformation, (4) the movement of atoms in the crystal is no more than the distance between two atoms in the crystal lattice, and (5) there are certain crystallographic relationships between martensite and the parent phase. A shear mechanism controls this transformation, wherein a large number of atoms move cooperatively and almost at the same time, as opposed to the atom-by-atom movement that occurs in diffusional transformations. This shear action produces two important characteristics of the martensite transformation: orientation relationships between parent and product phases and surface tilting around the martensite crystal. Due to the

absence of diffusion in the transformation, the composition of the parent austenite and product martensite are the same. Additionally, the martensite transformation is athermal—no thermal activation energy is associated with the transformation. While still a nucleation and growth mechanism, martensite forms through the diffusionless transformation of austenite. In general, a martensitic reaction can be defined as a mechanism for forming a new crystallographic structure that does not require atomic diffusion.

To form martensite, the cooling rate must be great enough to avoid the nose of the TTT diagram. Martensite starts forming when it is cooled below the M_s temperature and is completely transformed when it reaches the M_f temperature. Above the M_s temperature, martensite does not form, even at high cooling rates. The transformation only occurs at temperatures between the M_s and M_f. Because of matrix constraints, the width of the martensitic units is limited, and the transformation proceeds primarily by the successive nucleation of new crystals. This process occurs only on cooling to lower temperatures and is therefore independent of time. The transformation ceases when the steel falls below the M_f temperature. Some remaining austenite may still be present when the transformation stops, and it is referred to as retained austenite.

The martensitic transformation is effectively athermal because it occurs during cooling and begins when the sample is cooled below a particular temperature; the amount of the new phase that is formed forms depends on the temperature to which the sample is cooled rather than the time it spends at that temperature. If cooling is done quickly enough, structural rearrangement of atoms occurs by shear displacement over a small distance, on the order of approximately an interatomic spacing. This shear movement of atoms and phase growth occurs rapidly. It is not an instantaneous transformation, but it is quicker and distinct from the slower diffusion-controlled process in isothermal transformations.

The M_s temperature can be raised by the application of stress during transformation. This occurs because a crystal that forms during a martensitic transformation has a different shape and volume than that of the austenite from which it is forming. Therefore, if there is an applied stress available to achieve this shape change, the transformation will be accomplished more easily. If it can occur more easily, then it will require less thermodynamic driving force for it to occur, which means that the necessary degree of undercooling will be smaller. Thus, if an applied stress is locally oriented so that it helps the transformation to produce the shape change, martensite will be able to form at a higher temperature than for the unstressed condition. In general, tensile stresses are found to be more effective than compressive stresses, but rolling can have appreciable effects. The highest temperature to which the M_s temperature can be raised by applied stresses is defined as the M_d temperature. When the M_d temperature is above room temperature and the M_s is below room temperature, it is possible to retain

the austenite at room temperature and then to form some martensite by working the metastable austenite at room temperature.

As-quenched martensite has a very high strength but a very low fracture resistance or toughness. Therefore, almost all steels that are quenched to martensite are also tempered, or reheated to some temperature below A_1 in order to increase toughness. In tempered martensite, the carbide consists of small, chunky particles rather than platelets. These finely divided particles of cementite in tempered martensite provide strengthening and restore ductility, depending on the specific tempering temperature. In general, higher tempering temperatures result in lower strength but greater ductility.

The hardness of heat treated martensite is determined by its carbon content, as shown in Fig. 15.6. Martensite attains a maximum hardness of HRC 66 at carbon contents of 0.8 to 1.0 wt%. The reason that the hardness does not monotonically increase with carbon is that retained austenite starts forming when the carbon content is above approximately 0.4 wt%, and retained austenite is much softer than martensite.

Formation of Martensite in Steels. In a martensitic transformation process, large numbers of atoms experience cooperative movements with only a slight displacement of each atom relative to its neighbors. The fcc austenite transforms to a bct structure. This structure is essentially the same as the ferrite bcc structure, except that it has been distorted into a tetragonal structure due to the entrapment of carbon that did not have time to diffuse out and form cementite. Because the martensitic transformation

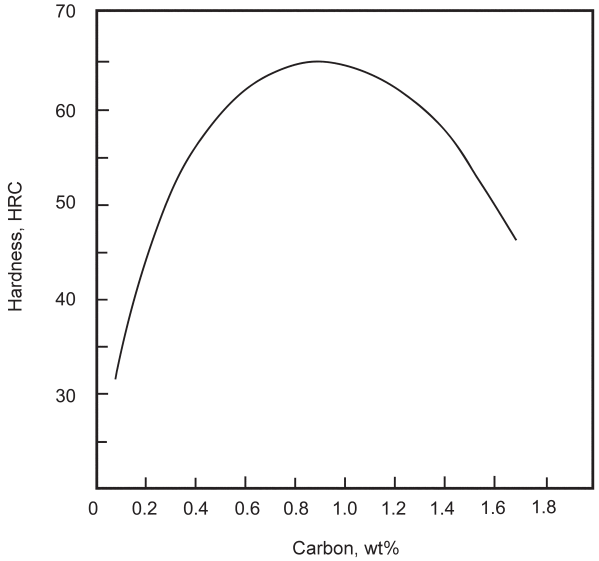

Fig. 15.6 Hardness versus carbon content for quenched steels. Source: Ref 15.4 as published in Ref 15.2

does not involve diffusion, it occurs almost instantaneously, approaching the speed of sound within the austenite matrix. All the carbon atoms remain as interstitial impurities in martensite, and as such, they constitute a supersaturated solid solution that is capable of rapidly transforming to other structures if heated to temperatures at which diffusion rates become appreciable. Because the bct crystal structure is less densely packed than the fcc structure of austenite, the transformation results in a volumetric expansion and a hardening of steel. As shown in Fig. 15.7, the *c*/*a* ratio of the tetragonal unit cell increases as the carbon content increases. To a good approximation, the variations in *c* and *a* are linear, with the *c* value increasing at a greater rate with increasing carbon contents than the rate at which the *a* parameter decreases.

Two adjacent fcc unit cells of austenite are shown in Fig. 15.8(a), in which a bct unit cell has been identified. The atoms identified in Fig. 15.8(a) have been isolated in the left-hand portion of Fig. 15.8(b). At this stage, the dimensions of the bct cell are still those derived from the austenite lattice parameter. The unit cell on the right-hand portion of Fig. 15.8(b) is that of martensite with lattice parameters *a* and *c*, corresponding to a given carbon content shown in Fig. 15.7. Note that a lattice deformation is required to produce martensite from austenite. This deformation was first identified by Bain and is referred to as the "Bain strain." As previously shown in Fig. 15.7, the Bain strain produces an expansion along the *c* axis and a contraction along the *a* axis.

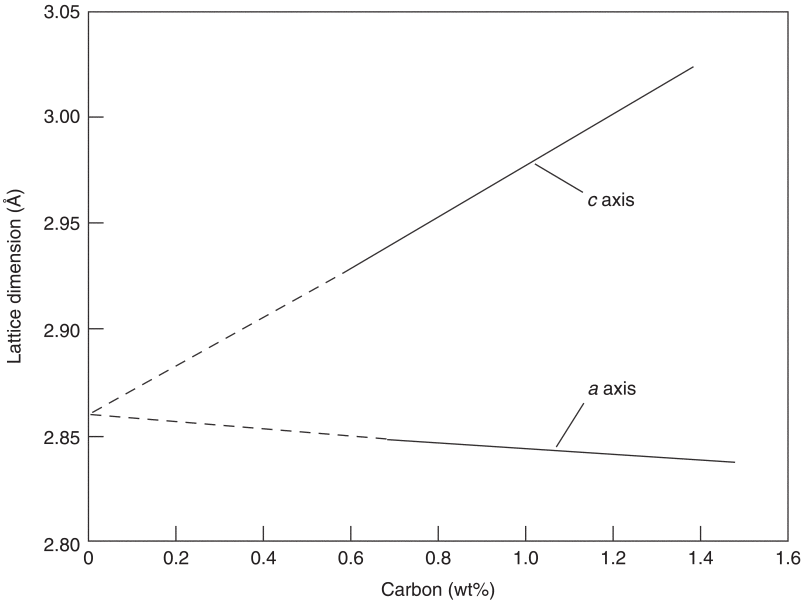

Fig. 15.7 Variation of *c*/*a* parameters with carbon content. Source: Ref 15.2

The formation of a martensitic crystal is shown schematically in Fig. 15.9. Shearing occurs parallel to a fixed crystallographic plane, termed the habit plane, and produces a uniformly tilted surface relief on a free surface. This mechanism involves shear displacement of iron atoms on specific planes, namely the {111} planes. In addition to the lattice distortion caused by the formation of the bct structure, the resulting martensite is simultaneously deformed because of the constraints created by maintaining an unrotated and undistorted habit plane within the bulk austenite. The deformation of martensite is referred to as a lattice invariant deformation,

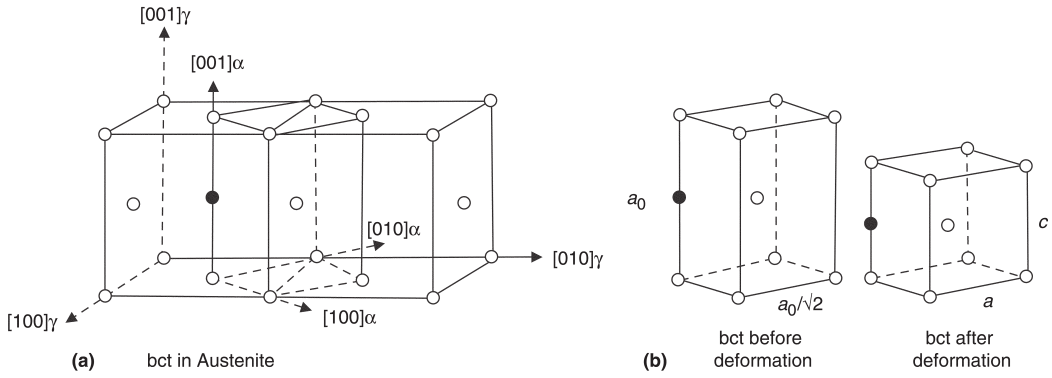

Fig. 15.8 Transformation from austenite to martensite. bct, body-centered tetragonal. Source: Ref 15.2

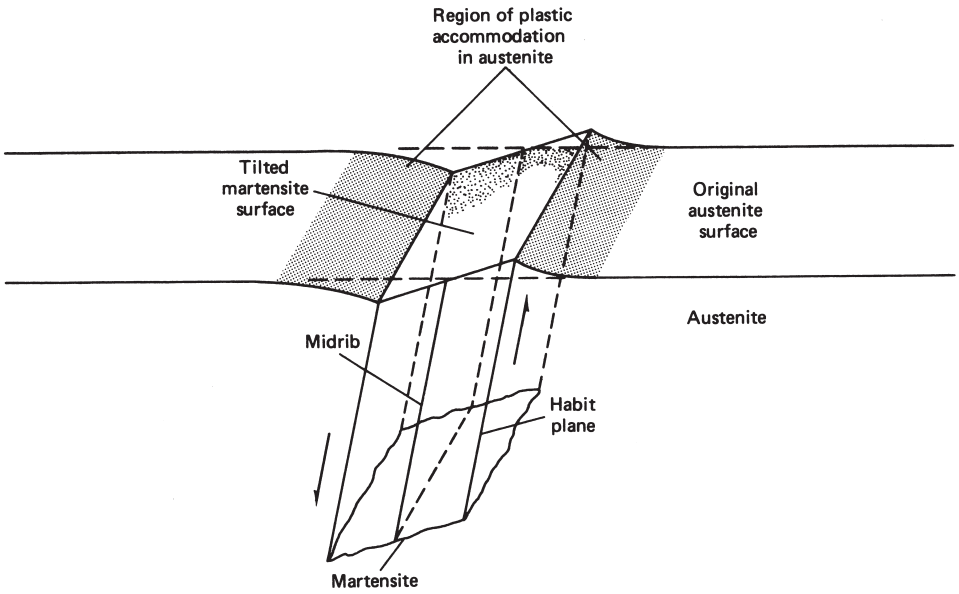

Fig. 15.9 Shear and surface tilting during martensite formation. Source: Ref 15.5 as published in Ref 15.2

and it produces a high density of dislocations or twins in martensite. The result is a bct crystal structure that is less densely packed than the fcc structure of austenite. Hence, the martensitic transformation results in a volumetric expansion and a hardening of steel. This fine structure, together with the carbon atoms trapped within the octahedral interstitial sites of the bct structure, produces the very high strength of as-quenched martensite.

Morphology of Martensite. In steels, there are two distinctly different microstructures that are found, depending on the carbon content of the steel (Fig. 15.10). For alloys containing less than approximately 0.6 wt% C, the martensite grains form as laths (i.e., long and thin plates) that form side by side and are aligned parallel to one another. Furthermore, these laths are grouped into larger structural entities, called blocks. The morphology of this lath or massive martensite is shown in Fig. 15.11. Lenticular, or plate, martensite is typically found in alloys containing greater than approximately 0.6 wt% C. With this structure, the martensite grains take on a needlelike (i.e., lenticular) or platelike appearance, which grows across the complete austenite grain shown in Fig. 15.12. Generally, plate martensite can be distinguished from lath martensite by its plate morphology with a central midrib. As the carbon content increases, twins begin to replace dislocations within the plates so that high-carbon martensite is composed mainly of twinned plates. The transformation is also associated with an appreciable volume increase, because it replaces the close-packed fcc structure with the more loosely packed bct structure. This transformation creates residual stresses that are related to the specific volume change, in addition to the strains due to the misfit of the interstitial solute atoms.

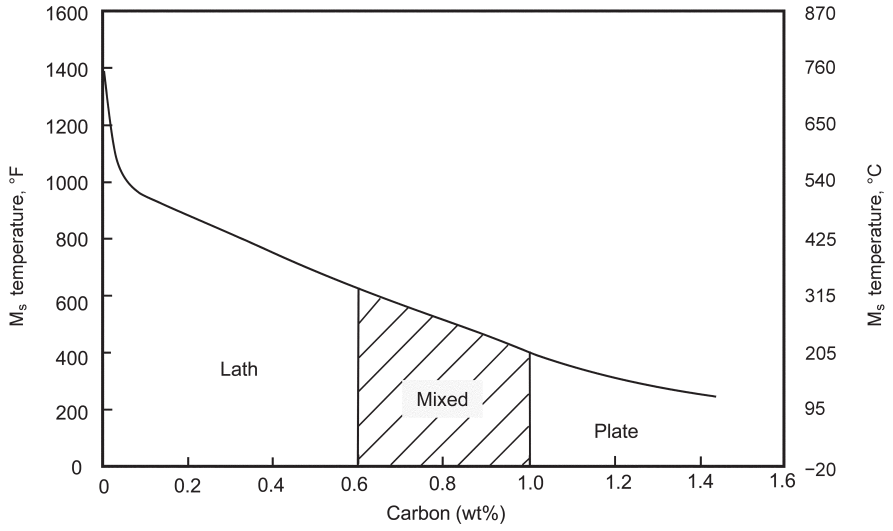

Fig. 15.10 Martensite morphology versus carbon content. Source: Ref 15.5 as published in Ref 15.2

At high carbon levels, these stresses can become so severe that the material cracks as the martensite forms. These cracks can range from small microcracks that require microscopy to be detected, to large cracks easily visible to the unaided eye. The cracks form during transformation when a growing plate impinges on an existing plate. Because of these microcracks, plate martensite is generally avoided in most applications. With carbon contents between 0.6 and 1.0 wt%, the martensite is a mixture of lath and plate morphologies.

Retained Austenite. Austenite starts transforming to martensite when it reaches the M_s temperature and continues to transform until the M_f temperature is reached. When the transformation ceases, some remaining austenite may still be present. When retained austenite is present, it is usually as small island grains surrounded by martensite (Fig. 15.13). Because martensite expands when it is formed, the remaining austenite is

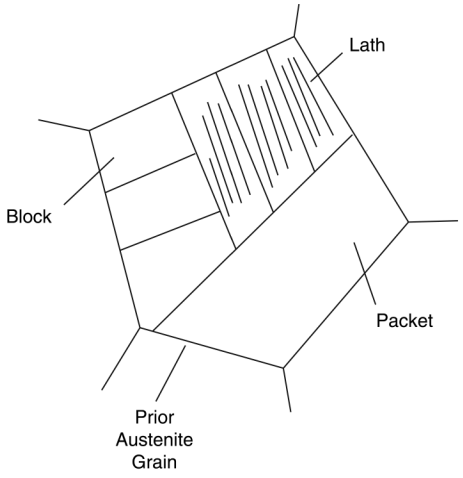

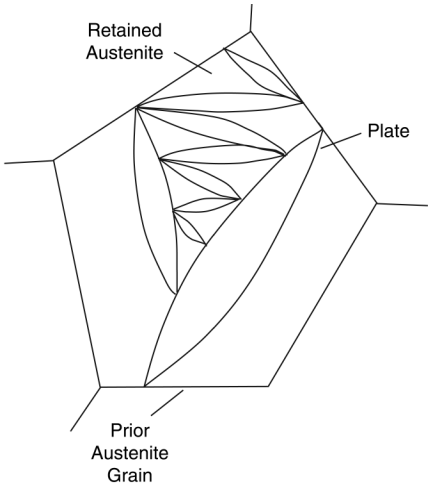

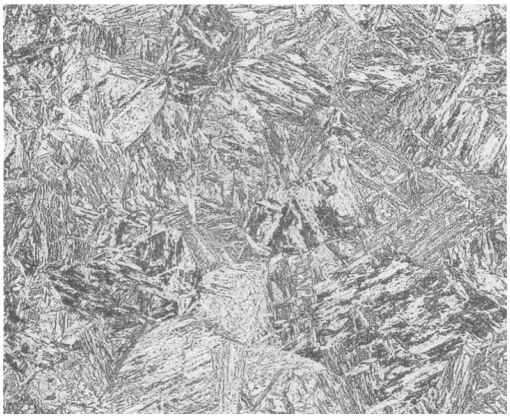

Fig. 15.11 Lath martensite. Source: Ref 15.4 as published in Ref 15.2

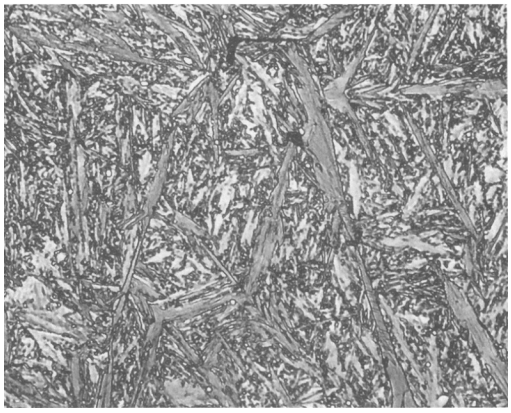

Fig. 15.12 Plate martensite. Source: Ref 15.4 as published in Ref 15.2

effectively pressurized from all sides. This makes it more difficult for it to expand, which it needs to do in order to transform into martensite. Because elastic deformation results in a volume expansion, impact-related stresses or other service loading conditions, as well as low-temperature exposure, can allow retained austenite to transform to martensite in service. Unless the service temperature is somewhat elevated, the new martensite will remain in an essentially untempered condition.

Carbon Content. The addition of carbon and other alloying elements causes significant changes in the isothermal transformation curves. As shown in Fig. 15.14, increasing amounts of carbon push the nose of the

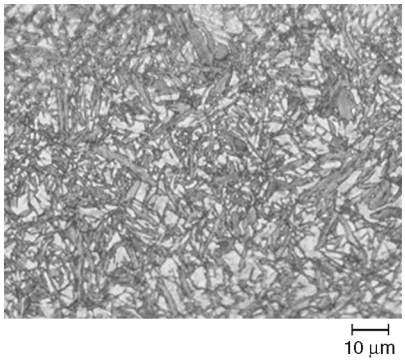

Fig. 15.13 Martensite microstructure with retained austenite (light areas). Source: Ref 15.6 as published in Ref 15.2

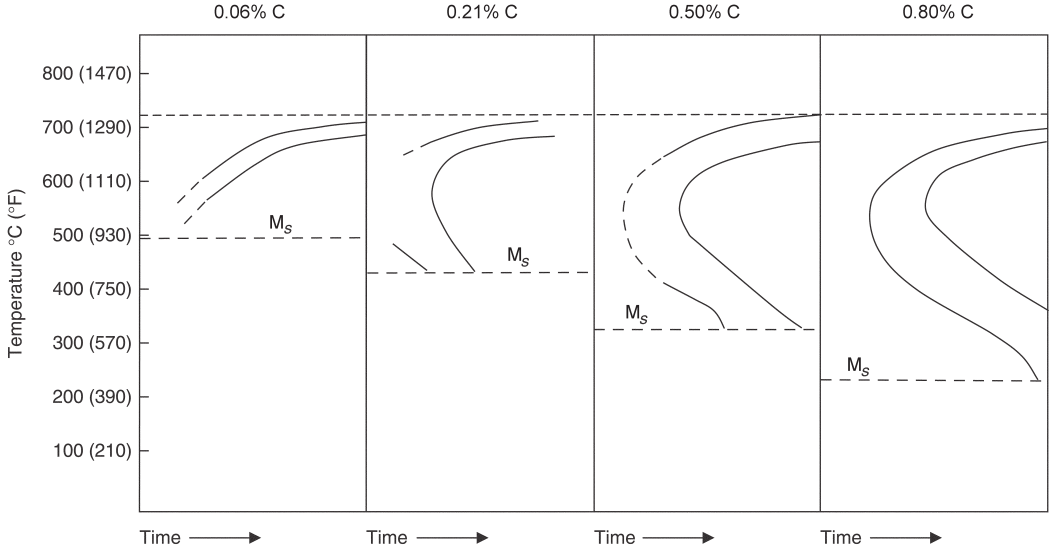

Fig. 15.14 Effect of carbon content on time-temperature-transformation (TTT) diagram. Source: Ref 15.2

TTT diagram to the right. The practical consequence is that steels with higher carbon contents can be hardened to form fully martensitic structures. For example, the steels containing 0.06 and 0.21 wt% C cannot be hardened to fully martensitic structures because there is not a quench fast enough to miss the nose of the TTT diagram. Thus, even with fast cooling, some pearlite will form. On the other hand, the steels containing 0.50 and 0.80 wt% C could, at least in thin sections, be hardened to fully martensitic structures. The main advantage of using substitutional alloying elements, rather than increasing carbon contents, is that the steel can be hardened to a greater depth without causing the brittleness associated with high carbon contents.

The M_s and M_s temperatures also depend on the carbon content of steel. When the carbon content is increased, carbide formation (Fe_3C) becomes more dominant under both isothermal and athermal conditions, and thus the M_s and M_f temperatures are lowered. Almost all other alloying elements also lower M_s. The reduction of the M_s and M_f temperatures, as function of carbon content and the alloying element manganese, are shown in Fig. 15.15. It is important to recognize that the martensitic transformation rarely goes to 100% completion. A small amount of the microstructure in a eutectoid plain carbon steel can be retained austenite. The amount of retained austenite varies with composition, being higher in steels containing high carbon contents and other alloying elements.

15.3 Tempering of Martensite in Steels

The martensitic structure that forms on rapid quenching of austenite in iron-carbon alloys is inherently brittle due to the large amount of lattice strain from supersaturation of carbon atoms, segregation of impurity atoms to grain boundaries, and residual stresses from the quench. This brittleness imparts high hardness to the steel but also results in low ductility and toughness. To regain ductility, the martensite may be tempered, which involves heating the steel to a temperature below the A_1 temperature

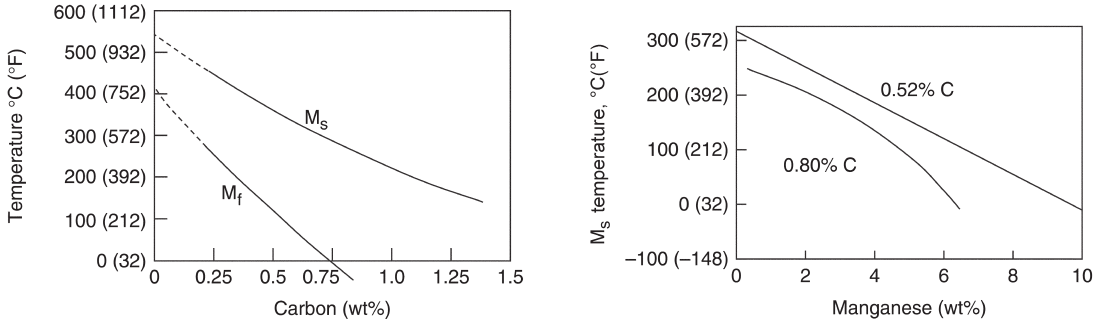

Fig. 15.15 Increasing carbon and alloy content lowers the M_s temperature. Source: Ref 15.2

(eutectoid temperature) and holding for varying amounts of time. Tempering will make the steel more ductile, but will also decrease the strength or hardness (Fig. 15.16).

The as-quenched structure of iron-carbon martensite is very unstable. Factors that contribute to this instability include supersaturation of the interstitial lattice sites with carbon atoms, strain energy from the fine structure (twins or dislocations), large amounts of interfacial energy from the laths or plates, and the presence of retained austenite. On reheating the as-quenched steel, the martensite will transform from the bct structure to a mixture of bcc iron (ferrite) and carbide (Fe_3C) precipitates. A typical tempered microstructure is shown in Fig. 15.17 for an Fe-0.2C alloy. Both the ferrite and the carbide will coarsen with increasing time and temperature, the driving force being the reduction of interfacial energy between the precipitates and the ferrite matrix.

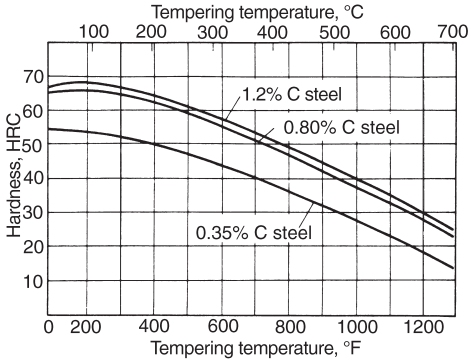

Fig. 15.16 Influence of increasing temperature (1 h) on decreasing the hardness of quenched carbon steels. Source: Ref 15.7 as published in Ref 15.3

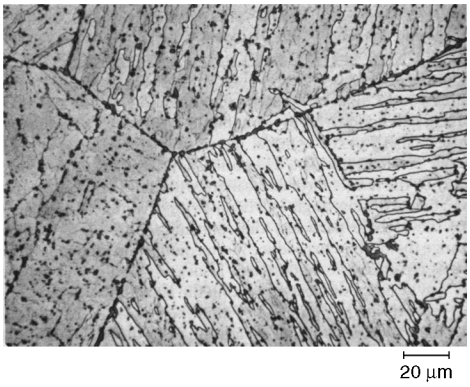

Fig. 15.17 Microstructure of lath martensite in an Fe-0.2C alloy after tempering at 700 °C (1290 °F) for 2 h. Nital etch. Original magnification: 500×. Source: Ref 15.8 as published in Ref 15.3

Early work on tempering of ferrous martensite outlined three distinct stages in the tempering process (Table 15.1). More recent research has been published that identifies the structural changes that occur during tempering (Table 15.2). The temperature ranges are approximate and are usually based on 1 h treatment times.

The fundamental mechanism responsible for tempering is a thermally activated process; both time and temperature are important variables in the tempering process. A tempering parameter is often used to describe the interaction between time and temperature: $T(20 + \log t) \times 10^{-3}$, where T is temperature in Kelvin, and t is time in hours. The tempering parameter makes it possible to create different time and temperature combinations to achieve a certain tempered structure.

The tempering time and temperature for a martensitic steel must be chosen carefully in order to obtain the required combination of strength and ductility. Overtempering may result in a loss of strength to such a degree

Table 15.1 Stages of the tempering process

Stage	Description	Temperature	
		°C	°F
I	Formation of a transition carbide (ε or η) and lowering of the carbon content of the matrix martensite to approximately 0.25% C	100–250	210–480
II	Transformation of retained austenite to ferrite and cementite	200–300	390–570
III	Replacement of the transition carbide and low-carbon martensite by cementite and ferrite	250–350	480–660

Source: Ref 15.8 as published in Ref 15.9

Table 15.2 Tempering reactions in steel

Temperature		Reaction and symbol (if designated)	Comments
°C	°F		
–40–100	–40–210	Clustering of 2–4 carbon atoms on octahedral sites of martensite; segregation of carbon atoms to dislocation boundaries	Clustering is associated with diffuse spikes around fundamental diffraction spots of martensite.
20–100	70–210	Modulated clusters of carbon atoms on (102) martensite planes (A2)	Identified by satellite spots around electron diffraction spots of martensite
60–80	140–180	Long period ordered phase with ordered carbon atoms arranged (A3)	Identified by superstructure spots in electron diffraction patterns
100–200	210–390	Precipitation of transition carbide as aligned 2 nm diam particles (T1)	Recent work identifies carbides as η (orthorhombic, Fe_2C); earlier studies identified the carbides as ε (hexagonal, $Fe_{24}C$).
200–350	390–660	Transformation of retained austenite to ferrite and cementite (T2)	Associated with tempered martensite embrittlement in low- and medium-carbon steels
250–700	480–1290	Formation of ferrite and cementite; eventual development of well-spheroidized carbides in a matrix of equiaxed ferrite grains (T3)	This stage now appears to be initiated by χ-carbide formation in high-carbon Fe-C alloys.
500–700	930–1290	Formation of alloy carbides in Cr-, Mo-, V-, and W-containing steels. The mix and composition of the carbides may change significantly with time (T4).	The alloy carbides produce secondary hardening and pronounced retardation of softening during tempering or long-time service exposure near 500 °C (930 °F).
350–550	660–1020	Segregation and cosegregation of impurity and substitutional alloying elements	Responsible for temper embrittlement

Source: Ref 15.10 as published in Ref 15.9

that the component is no longer useful for the intended application. The amount of softening that occurs with tempering can be altered with the addition of alloy elements. Softening occurs by the diffusion-controlled coarsening of cementite. Strong carbide formers, such as chromium, molybdenum, and vanadium, will reduce the rate of coarsening and thus minimize the amount of softening. Additionally, at higher tempering temperatures, these elements may themselves form carbides, leading to an increase in overall hardness; this is termed secondary hardening.

Different morphologies of tempered martensite will form depending on the heat treatment and the original martensite microstructure. It has been observed that packets of aligned laths in low-carbon martensites will transform into large acicular grains, as shown in Fig. 15.18(a–c). In higher-carbon plate martensites, large martensite plates transform to equiaxed grains on tempering (Fig. 15.19a–c). Additionally, these figures show how the carbides form on the grain boundaries and how both the ferrite grains and the carbides coarsen. When tempering procedures are not carefully

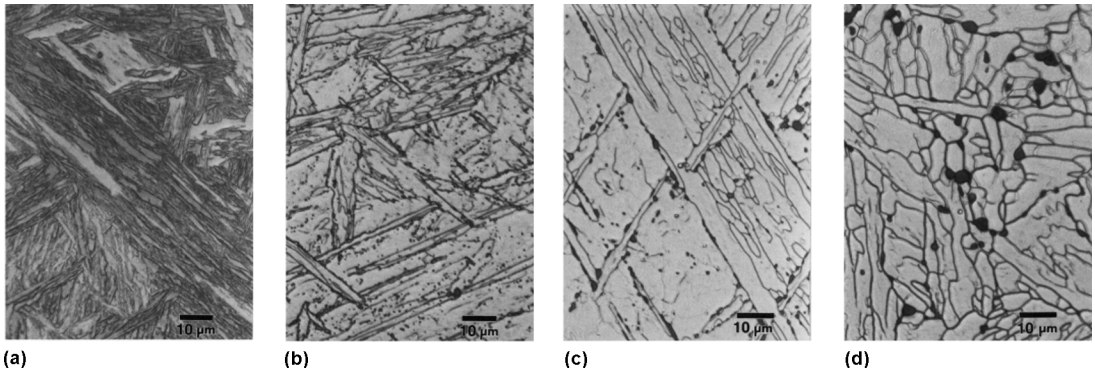

Fig. 15.18 Fe-0.2C alloy (a) in the water-quenched condition, followed by tempering at 690 °C (1275 °F) for (b) 1.5 × 10^3 s, (c) 1.03 × 10^4 s, and (d) 6.05 × 10^5 s. Source: Ref 15.11 as published in Ref 15.9

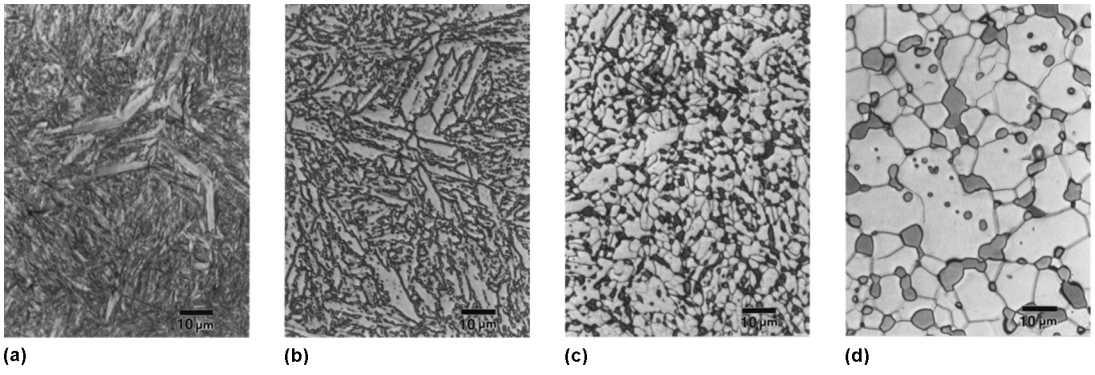

Fig. 15.19 Fe-1.2C alloy (a) in the water-quenched condition, followed by tempering at 690° C (1275 °F) for (b) 1.5 × 10^3 s, (c) 1.03 × 10^4 s, and (d) 6.05 × 10^5 s. Source: Ref 15.11 as published in Ref 15.9

chosen, spheroidization can occur, wherein the Fe_3C coalesces to form spheroid particles. The microstructures in Fig. 15.18(d) and 15.19(d) are both spheroidized.

The change in morphology of tempered martensite, as shown in Fig. 15.18 and 15.19, provides an explanation for the change in mechanical properties of martensite from the as-quenched to the as-tempered form. As-quenched martensite has a very high density of dislocations, leading to high hardness and high work hardenability due to dislocation tangles. Tempering martensite causes the carbides to coarsen, increasing their average size while simultaneously decreasing their total population. Dislocation interactions with carbides is thus reduced significantly on tempering, and work hardenability is reduced. This effect is depicted in Fig. 15.20, which shows true-stress/true-strain curves for an as-quenched and a tempered lath martensite. The work-hardening rate, indicated by the slope of the stress-strain curve, is much higher for the as-quenched steel than for the tempered steel.

15.4 Nonferrous Martensite

Formation of the martensite structure in nonferrous systems occurs by the same diffusionless displacive transformation mechanisms described for ferrous systems. Macroscopic deformation resulting from martensitic transformations will result in upheaval on the surface of polished specimens, as shown in Fig. 15.21. If there are no obstructions from a diffusion-controlled transformation (as there are for iron-carbon alloys), the martensitic surface relief formed on cooling can be removed by heating to temperatures above the start temperature of the parent phase. The

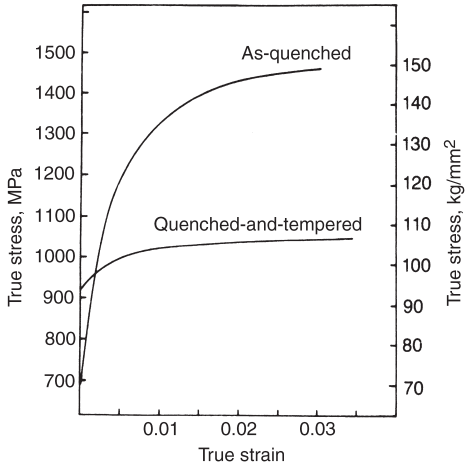

Fig. 15.20 True-stress/true-strain curves for Fe-0.2C as-quenched and quenched-and-tempered lath martensite with packet size of 8.2 μm. Source: Ref 15.8 as published in Ref 15.9

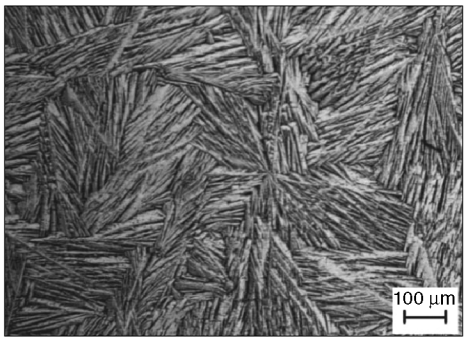

Fig. 15.21 Relief effects observable on a polished surface of Ni-50.3Ti-2W are characteristic of the martensitic transformation. Water quenched from 550 °C (1020 °F). Source: Ref 15.12 as published in Ref 15.13

transformation hysteresis is thus defined by the difference between the forward and reverse transformation temperatures. Reversibility of the transformation is typical of nonferrous systems that undergo the martensitic transformation.

Nonferrous martensitic transformations exhibit a characteristic platelike microstructure (in most cases), such that one dimension of the martensite region is much smaller than the other two. Viewed in cross section on a scale observable in light optical microscopy, these plates have a needle shape that can traverse entire grains or form various internal arrangements within grains (Fig. 15.22). Macroscopic shape changes associated with the martensitic transformation from parent to product phase, a result of the Bain strain and lattice-invariant deformation, induce stress in the surrounding matrix. Lenticular-shaped martensite plates are often observed, believed to form due to an increasing elastic stress surrounding the plate during formation. The lenticular plate shapes, and martensite plate groupings in various orientations (variants), have been found to reduce the constraining elastic stress through accommodation of the macroscopic shape changes (Fig. 15.23).

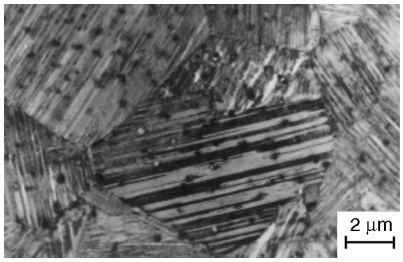

Fig. 15.22 Transmission electron microscopy image of martensite present in Cu-11.4Al-5Mn-2.5Ni-0.4Ti (wt%). Melt spun at a wheel speed of 6.5 m/s. Precipitates of Cu_2AlTi are visible, dispersed evenly across the different grains. Source: Ref 15.14 as published in Ref 15.13

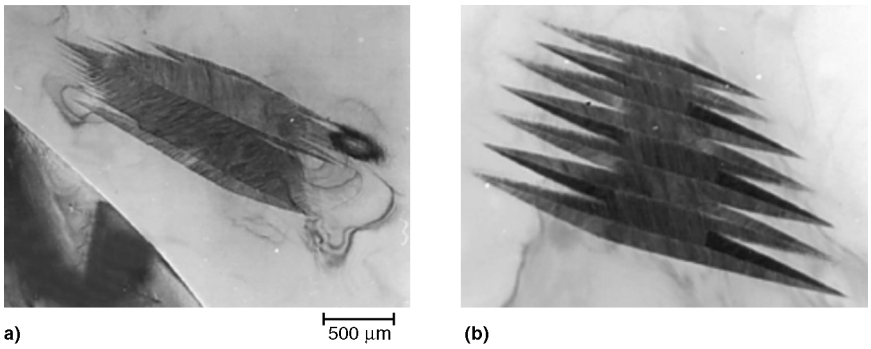

Fig. 15.23 Transmission electron microscopy images of splat-cooled Ni-37.5Al (at.%) showing accommodating martensite groupings. Source: Ref 15.15 as published in Ref 15.13

Historically, martensitic transformations in metal alloys (specifically steel) have been studied the most, but recent attention has also been given to ceramic, mineral, and organic systems that develop martensite structures. Table 15.3 lists different metal alloy systems that undergo martensitic transformations, along with specific alloys or compounds and the general changes in crystal structure for such systems.

Nonferrous martensite in metal alloys has been studied extensively. In metallic systems, nonferrous martensite generally occurs in substitutionally alloyed systems that demonstrate small transformation strains and a small transformation hysteresis. The macroscopic deformation from the resultant transformation from one crystal structure to another can be observed from the surface relief and in the plate morphology that the martensite phase usually assumes. Substructure of the martensite plates can be characterized with the use of transmission electron microscopy (TEM). Stacking faults, twins, and dislocations are commonly observed within martensite plates. Twinning deformation or slip along the shear planes can accommodate structural transformations that would otherwise result in a significant shape change. Their presence and frequency within the martensite phase is dependent on the alloy system and composition.

Table 15.3 Metal alloy martensite transformations for selected systems

Metal alloy	General parent crystal structure	General martensite crystal structure
Ag alloys (Ag-Cd, Ag-Ge, Ag-Zn)	bcc	3R, 9R, 2H
Au alloys (Au-Cd, Au-Cu-Zn, Au-Zn)	bcc	3R, 9R, 2H
Co alloys (Co, Co-Be, Co-Ni)	fcc	hcp
Cu alloys (Cu-Al, Cu-Al-Ni, Cu-Sn, Cu-Zn)	bcc	3R, 9R, 2H
In alloys (In-Tl, In-Cd)	fcc	fct
Li alloys (Li, Li-Mg)	bcc	hcp
Ni alloys (Ni-Al, Ni-Ti)	bcc	3R, 9R, 2H
Mn alloys (Mn-Cu, Mn-Ni)	fcc	fct
Ti alloys (Ti, Ti-Cu, Ti-Mn, Ti-Mo, Ti-V)	bcc	hcp
Zr alloys (Zr, Zr-Mo, Zr-Nb)	bcc	hcp

bcc, body-centered cubic; fcc, face-centered cubic; hcp, hexagonal-close packed; fct, face-centered tetragonal. Source: Ref 15.13

Martensitic transformations in metallic systems can be grouped into three categories:

- In the first group, allotropic transformations of the solvent atoms create the martensite product. Martensitic transformations in cobalt, titanium, zirconium, hafnium, and lithium alloys belong to this group. Cobalt and alloys undergo a fcc to hexagonal close-packed (hcp, ε) martensitic transformation. Cobalt and cobalt-nickel alloys can therefore have a high measure of stacking faults within the martensite plates. Titanium, zirconium, hafnium, and lithium alloys generally transform from bcc (β phase) to hcp structures, although fcc and orthorhombic martensite structures have been reported in some titanium and zirconium alloys. Lath morphologies have been observed in some of the titanium and zirconium alloys as well. Twins are commonly found in the plate martensite form of these alloys, while stacking faults are commonly observed in lath martensite.
- Copper, gold, and silver alloys belong to the β phase Hume-Rothery alloy group, whose parent phase is a bcc structure. Nickel alloys such as nickel-aluminum and nickel-titanium (~50 to 50 ratio) are also part of this alloy group, with a bcc parent phase. Because the transformations are diffusionless and lattice correspondence is maintained, order or disorder present in the parent phase is transferred to the martensite phase. Often a superlattice structure is present that is then converted to the martensite product. These alloys all belong to the second category, marking a weak first-order transformation with an intermediate stability of the martensite phase at temperatures above the M_s temperature. Alloys used in shape memory applications are found in this category.
- The third category of martensitic transformations belongs to second-order transformations (very weak first order) that have a larger mechanical instability of the martensite phase. First-order phase transformations are those phase transformations for which the first derivative of Gibbs free energy with respect to temperature and pressure are discontinuous at the equilibrium transformation temperature. Second-order phase transformations have continuous first derivatives but have discontinuous second derivatives of Gibbs free energy with respect to temperature and pressure. The fcc to face-centered tetragonal (fct) martensitic transformation of manganese and indium alloys falls into this category.

15.5 Shape Memory Alloys

Shape memory alloys (SMA) are a group of alloys that have the ability to return to some previously defined shape or size when subjected to an appropriate thermal cycle. Generally, these materials can be plastically

deformed at relatively low temperature and, on exposure to some higher temperature, will return to their shape prior to the deformation. Materials that exhibit shape memory only on heating are referred to as having a one-way shape memory. Some materials also undergo a change in shape on recooling. These materials are said to have a two-way shape memory. Nitinol (50Ti-50Ni) is one of the best known and most useful of the SMAs. Nitinol has been used for blood clot filters in medical applications, hydraulic couplings for aircraft, force actuators, proportional control devices, and superelastic eyeglass frames.

A SMA can be further defined as one that yields thermoelastic martensite. In this case, the alloy undergoes a martensitic transformation of a type that allows the alloy to be deformed by a twinning mechanism below the transformation temperature. The deformation is then reversed when the twinned structure reverts on heating to the parent phase. The martensitic transformation that occurs in SMAs yields a thermoelastic martensite that develops from a high-temperature austenite phase with long-range order. The transformation does not occur at a single temperature but over a range of temperatures that varies with each alloy system. The usual way of characterizing the transformation and naming each point in the cycle is shown in Fig. 15.24. Most of the transformation occurs over a relatively narrow temperature range, although the beginning and end of the transformation during heating or cooling actually extends over a much larger temperature range. The transformation also exhibits a hysteresis in that the transformation on heating and on cooling does not overlap. This transformation hysteresis varies with the alloy system.

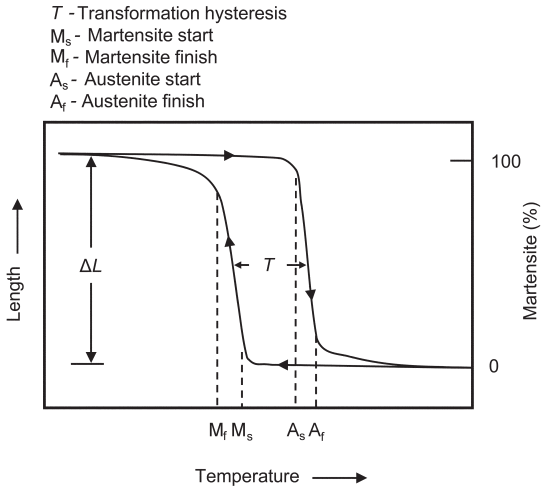

Fig. 15.24 Typical transformation-versus-temperature curve for a shape memory alloy. Source: Ref 15.16 as published in Ref 15.2

15.6 Bainitic Structures

At temperatures between those at which the eutectoid transformation of austenite to pearlite and the transformation of austenite to martensite occur, a variety of unique microstructures may form in carbon steels. Davenport and Bain showed by careful light microscopy that the microstructures formed at such intermediate temperatures were quite different from those of pearlite and martensite, and in honor of Edgar C. Bain, his colleagues termed the unique microstructures bainite. The schematic TTT diagram in Fig. 15.25 clearly shows the intermediate temperature range, between those of pearlite and martensite, for bainite formation.

Steels with carbon contents other than the eutectoid composition would of course have regions of proeutectoid phase formation at temperatures above that of pearlite formation. The schematic diagram of Fig. 15.25 shows a well-defined TTT range for bainite formation. Such a well-defined range of bainite transformation is characteristic of low-alloy steels, especially on continuous cooling. In plain carbon steels, the transformation regions for proeutectoid ferrite/pearlite and bainite are more continuous and even overlap with decreasing temperature. In alloy steels, alloying elements may even cause the arrest of bainite transformation, causing incomplete transformation at intermediate temperatures. The extreme effects of alloy-

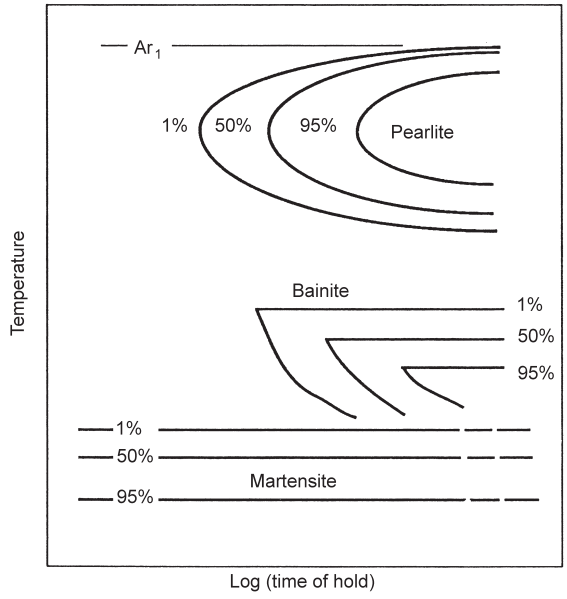

Fig. 15.25 Schematic TTT diagram for a steel with well-defined pearlite and bainite formation ranges. Source: Ref 15.17 and 15.18 as published in Ref 15.19

ing on bainitic transformation, ranging from those in plain carbon steels to those in alloyed steels, are shown schematically in the TTT diagrams in Fig. 15.26.

Austempering is the interrupted quenching process that is used to form a bainitic structure. The part is quenched into a salt bath above the M_s temperature. However, it is allowed to remain at that temperature until the transformation to bainite is complete (Fig. 15.27). Because austempering is an interrupted quenching process that produces bainite rather than martensite, parts can usually be produced with less dimensional change

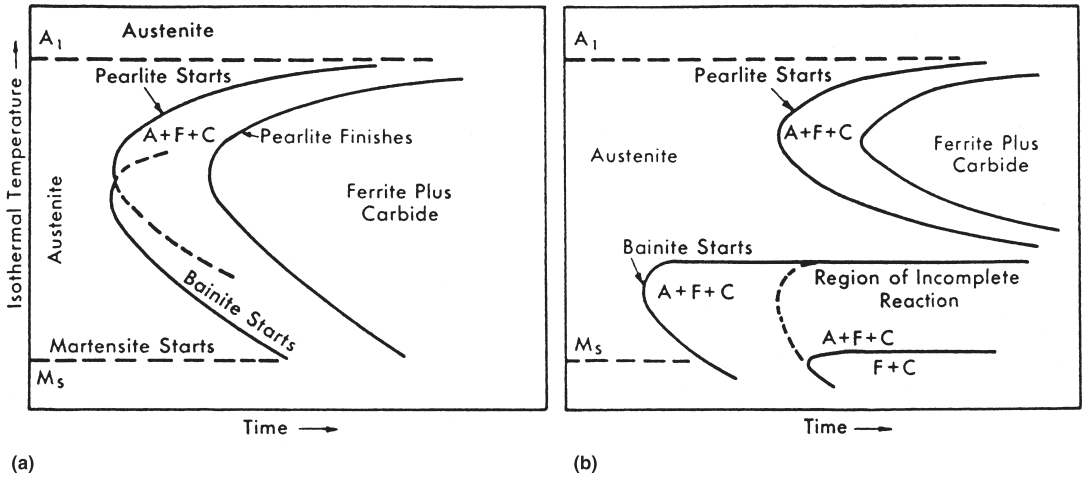

Fig. 15.26 Schematic TTT diagrams for (a) plain carbon steel with overlapping pearlite and bainite transformation and (b) alloy steel with separated bainite transformation and incomplete bainite transformation. Source: Ref 15.20 and 15.21 as published in Ref 15.19

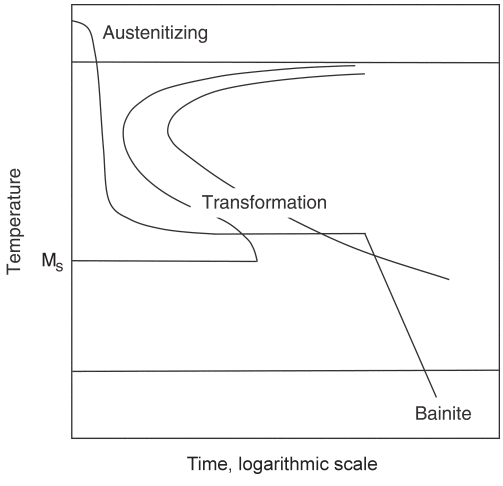

Fig. 15.27 Typical austempering heat treatment. Source: Ref 15.2

than is typical through conventional quenching and tempering. In addition, austempered parts do not normally require a tempering operation. A typical austempering cycle would be to heat to a temperature within the austenitizing range (790 to 910 °C, or 1450 to 1675 °F), quench in a salt bath maintained at a constant temperature, usually in the range of 260 to 400 °C (500 to 750 °F), allowing time for the austenite to isothermally transform to bainite, and then air cool to room temperature. For true austempering, the metal must be cooled from the austenitizing temperature to the temperature of the austempering bath fast enough so that no transformation of austenite occurs during cooling, and then held at bath temperature long enough to ensure complete transformation of austenite to bainite. Austempering offers several potential advantages, including increased ductility, toughness, and strength at a given hardness, reduced distortion, and the ability to heat treat steels to a hardness of HRC 35 to 55 without having to temper.

Bainite Transformation Start Temperatures. The temperature at which bainite transformation starts is referred to as the B_s temperature, and several empirical equations that show the effect of alloying elements on B_s have been determined. The equation for B_s as a function of composition (in wt%) for hardenable low-alloy steels containing from 0.1 to 0.55% C is:

$$B_s\ (°C) = 830 - 270(\%C) - 90(\%Mn) - 37(\%Ni) - 70(\%Cr) - 83(\%Mo) \quad \text{(Eq 15.1)}$$

Equation 15.2 is applicable for low-carbon bainitic steels (containing between 0.15 and 0.29% C) for high-temperature applications in the electric power industry. Compositions of the alloying elements are in wt%.

$$B_s\ (°C) = 844 - 597(\%C) - 63(\%Mn) - 16(\%Ni) - 78(\%Cr) \quad \text{(Eq 15.2)}$$

Bainite versus Ferritic Microstructures. Bainitic microstructures take many forms. In medium- and high-carbon steels, similar to pearlite, bainite is a mixture of ferrite and cementite and is therefore dependent on the diffusion-controlled partitioning of carbon between ferrite and cementite. However, unlike pearlite, the ferrite and cementite are present in nonlamellar arrays. Similar to martensite, the ferrite of bainitic microstructures may appear as acicular crystals, similar to the laths and plate-shaped crystals of martensite. Bainite is grouped into two types, upper and lower bainite, depending on the temperature range at which the transformation occurs. The effect of steel carbon content on transition temperatures between upper and lower bainite formation is shown in Fig. 15.28. In low-carbon steels, at intermediate transformation temperature ranges, austenite may transform only to ferrite, resulting in two-phase microstructures of ferrite and retained austenite. Although some features of the intermediate ferritic

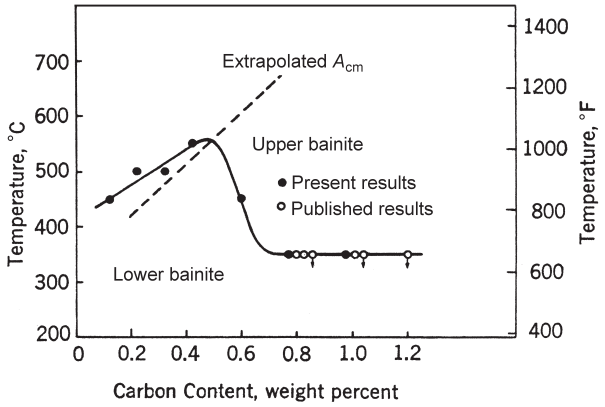

Fig. 15.28 Effect of steel carbon content on the transition temperature between upper and lower bainite. Source: Ref 15.22 as published in Ref 15.19

microstructures are similar to those of the classical bainites, the absence of cementite in ferritic microstructures makes possible a clear differentiation of intermediate-temperature-transformation products of austenite decomposition.

According to a microstructural definition of bainite in steels as a nonlamellar ferrite-cementite product of austenite transformation, six morphologies of cementite-ferrite microstructures considered to be bainite are shown schematically in Fig. 15.29. Upper and lower bainites are the most common forms found in medium-carbon steel. However, in the absence of cementite, intermediate-temperature-transformation products of austenite fall in the category of ferrites.

Upper bainite forms in the temperature range just below that at which pearlite forms, typically below 500 °C (932 °F). Figure 15.30 shows light micrographs of upper bainite formed by holding 4360 steel at 495 and 410°C (920 and 770°F). The bainite appears dark and the individual ferritic crystals have an acicular shape. The bainitic transformation was not completed during the isothermal holds at the temperatures noted, and therefore the light etching areas are martensite that formed in untransformed austenite on quenching after the isothermal holds. The bainite appears dark (i.e., has low reflectivity) because of roughness produced by etching around the cementite particles of the bainitic structure. The cementite particles, however, are too fine to be resolved in the light microscope.

The feathery appearance of the clusters of ferrite crystals is clearly shown in the light micrographs and is sometimes an important identifying feature of upper bainite. Upper bainite microstructures develop by packets or sheaves of parallel ferrite crystals growing across austenite grains, producing a blocky appearance. This latter characteristic of upper bainite in 4150 steel transformed at 460 °C (860 °F) is shown in Fig. 15.31.

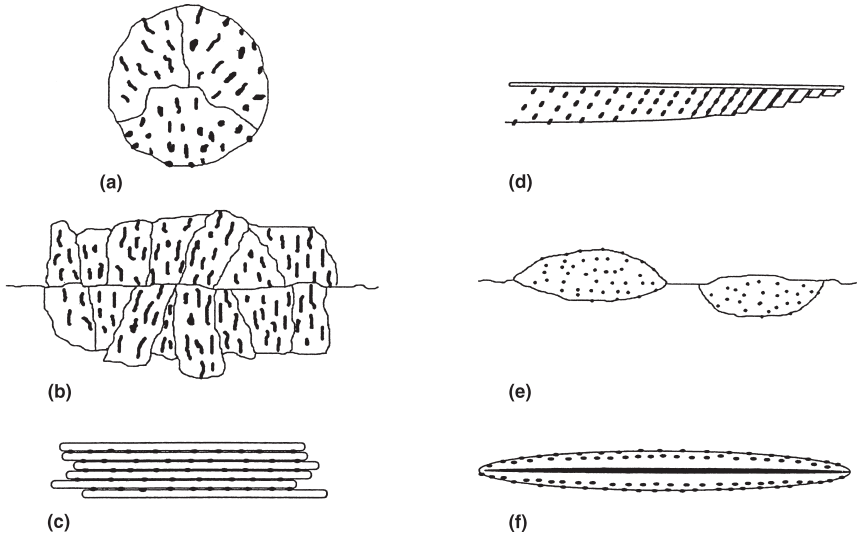

Fig. 15.29 Schematic illustrations of various ferrite (white)-cementite (black) microstructures defined as bainite according to Aaronson et al. (a) Nodular bainite. (b) Columnar bainite. (c) Upper bainite. (d) Lower bainite. (e) Grain-boundary allotromorphic bainite. (f) Inverse bainite. Source: Ref 15.20 as published in Ref 15.19

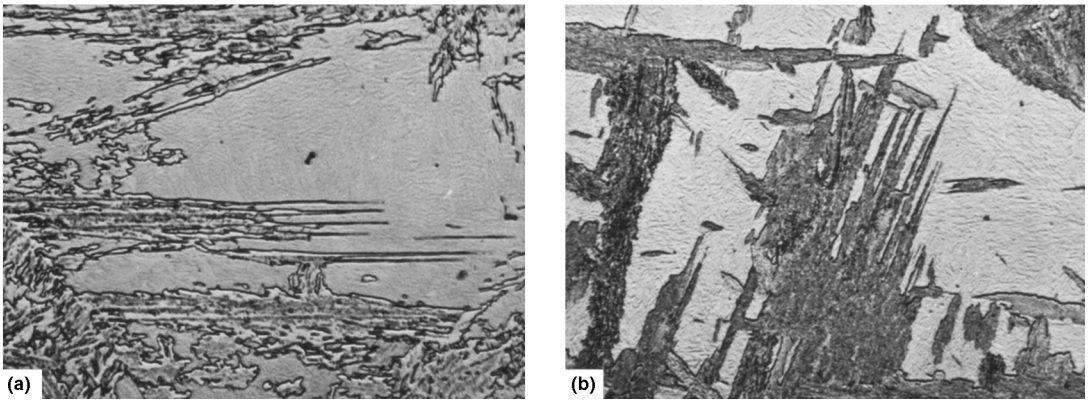

Fig. 15.30 Upper bainite in 4360 steel isothermally transformed at (a) 495 °C (920 °F) and (b) 410 °C (770 °F). Light micrographs, picral etch. Original magnification: 750×. Source: Ref 15.23 as published in Ref 15.19

The cementite particles of upper bainite form between ferrite crystals in austenite enriched by carbon rejection from the growing ferrite crystals.

Figure 15.32 is a thin-foil TEM micrograph that shows interlath cementite in a 4360 steel transformed to bainite at 495 °C (920 °F). The carbide particles, compared with those that are present in lower bainite, are relatively coarse and appear black and elongated. In some steels, especially those with high silicon content, cementite formation is retarded. As a result, the carbon-enriched austenite between the ferrite laths is quite stable and

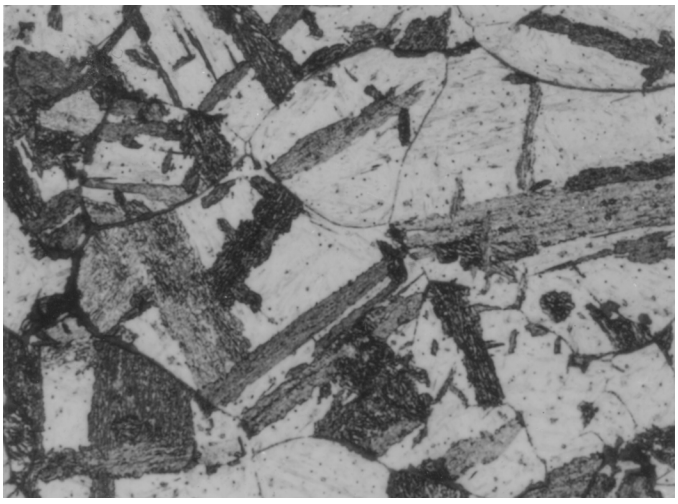

Fig. 15.31 Upper bainite (dark rectangular areas) in 4150 steel transformed at 460 °C (860 °F). Original magnification: 500×. Courtesy of Florence Jacobs, Colorado School of Mines. Source: Ref 15.19

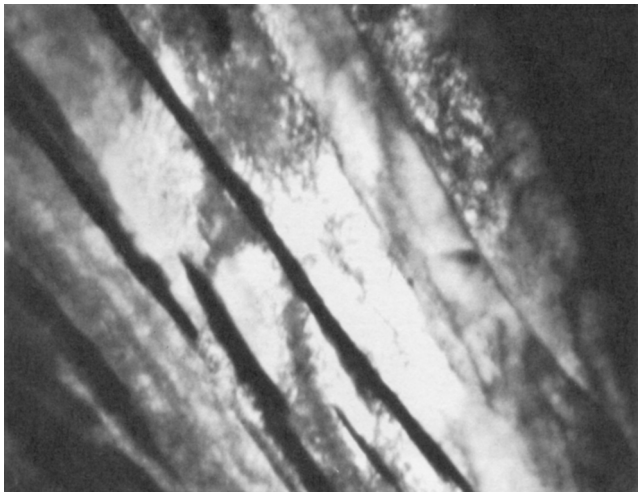

Fig. 15.32 Carbide particles (dark) formed between ferrite crystals in upper bainite in 4360 steel transformed at 495 °C (920 °F). Transmission electron micrograph. Original magnification: 25,000×. Source: Ref 15.23 as published in Ref 15.19

is retained during transformation and at room temperature. Figure 15.33 shows retained austenite in bainite formed at 400 °C (752 °F) in a steel containing 0.6% C and 2.0% Si. The austenite in this TEM image appears gray.

Lower Bainite. An example of lower bainite, obtained from a specimen of 4360 steel partially transformed at 300 °C (570 °F), is shown in Fig. 15.34. Again, the bainite etches dark, and the white-etching matrix is

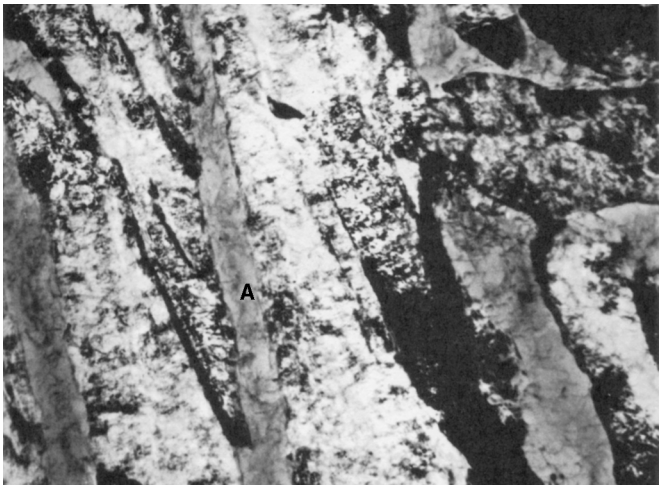

Fig. 15.33 Retained austenite (gray, marked with A) between ferrite laths of upper bainite in 0.6% C steel containing 2.0% Si and transformed at 400 °C (750 °F). Transmission electron micrograph. Original magnification: 40,000×. Source: Ref 15.23 as published in Ref 15.19

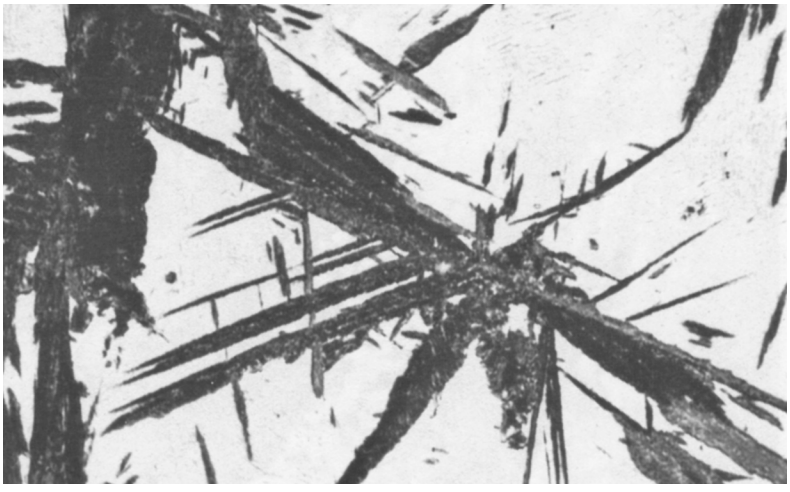

Fig. 15.34 Lower bainite in 4360 steel transformed at 300 °C (570 °F). Original magnification: 750×. Source: Ref 15.23 as published in Ref 15.19

martensite formed on cooling in the austenite not transformed to bainite at 300 °C (570 °F).

Lower bainite is composed of large ferrite plates that form nonparallel to one another and, analogous to plate martensite microstructures, is often characterized as acicular. The carbides in the ferrite plates of lower bainite are responsible for its dark etching appearance but are much too fine to be resolved in the light microscope.

Figure 15.35 shows the very fine carbides that have formed in ferrite of lower bainite in 4360 steel transformed at 300 °C (570 °F). The fine carbides typically make an angle of approximately 60° with respect to the long axis of the matrix ferrite crystal. In contrast to upper bainite, fine carbides form within ferrite crystals, rather than between plates, and are significantly finer than the interlath carbides of upper bainite. A variant of lower bainite is termed lower bainite with midrib and forms isothermally at lower temperatures, 150 to 200 °C (300 to 350 °F), than the temperatures at which conventional lower bainite forms, 200 to 350 °C (390 to 660 °F). Figure 15.36 shows light and TEM micrographs of lower bainite

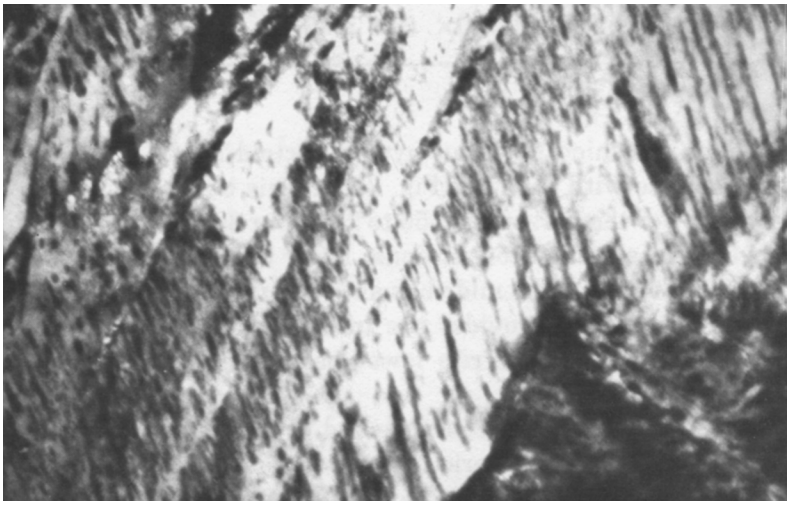

Fig. 15.35 Lower bainite with fine carbides within ferrite plates in 4360 steel transformed at 300 °C (572 °F). Transmission electron micrograph. Original magnification: 24,000×. Source: Ref 15.23 as published in Ref 15.19

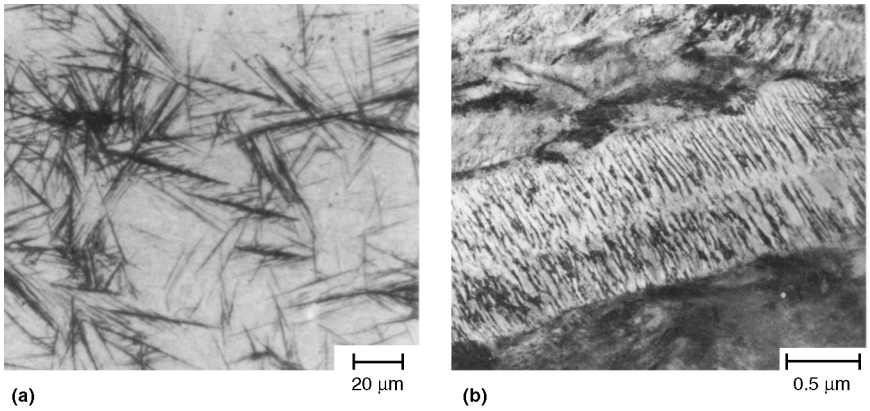

Fig. 15.36 Lower bainite with midribs in a 1.1% C steel transformed at 190 °C (374 °F) for 5 h. (a) Light micrograph. (b) Transmission electron micrograph. Courtesy of H. Okamoto, Tottori University. Source: Ref 15.19

with midrib in a 1.1% C steel transformed at 190 °C (370 °F). The midrib is an isothermally formed thin plate of martensite that provides the interface at which the two-phase carbide-ferrite lower bainitic structure forms.

Bainite Formation Mechanisms. The fact that the classical bainites consist of ferrite and nonlamellar distributions of cementite attests to the need for carbon diffusion during some stage of bainite transformation. However, the relatively low temperatures at which bainites form severely restrict iron atom diffusion. The latter feature of the transformation of austenite to bainite has led to two quite different views of ferrite nucleation in bainite. The first view states that the first-formed ferrite is formed by a diffusionless shear or martensitic transformation. The second view states that the first-formed ferrite nucleates and grows by a ledge-type mechanism where short-range iron atom rearrangement can take place at ledges in the ferrite-austenite interface. There is scientific and experimental support for both sides of the argument about the nucleation and growth mechanisms of bainite.

The empirical B_s equations noted earlier reflect the strong effect of alloying elements on the start of bainitic transformation. Coupled with this characteristic of steels with prominent bainite transformations is the presence of a pronounced bay or region of very sluggish transformation in TTT diagrams. These regions correspond to the temperature ranges that show the marked separation of the transformation curves for pearlite and bainite in Fig. 15.25. An example of such a bay is shown in the isothermal TTT diagram for 4340 steel (Fig. 15.37).

Such bays correlate with the presence of substitutional alloying elements that may partition to or from ferrite and concentrate at austenite-ferrite interfaces, creating a solute drag or significant restraining force on the formation of bainitic ferrite. As noted relative to Fig. 15.26, the isothermal transformation of austenite to bainite may be severely retarded. This phenomenon is referred to as stasis and is also discussed in terms of atom partitioning and solute drag at austenite-ferrite interfaces.

The distribution of very fine carbides in plates of lower bainite suggests that a ferrite crystal has initially formed, perhaps by a martensitic mechanism, and as a consequence of the supersaturation of the ferrite with carbon, fine carbides precipitate within the ferrite. Another explanation for the formation of lower bainite is that a unit of lower bainite forms by a four-step process: (1) precipitation of a nearly carbide-free ferrite spine; (2) sympathetic nucleation of secondary plates of ferrite, usually on only one side of and at an angle of approximately 55 to 60° to the initiating spine; (3) precipitation of carbides in austenite at α:γ boundaries, forming gaps between adjacent secondary (ferrite) plates; and (4) an annealing process in which the gaps are filled in with further growth of ferrite and additional carbide precipitation.

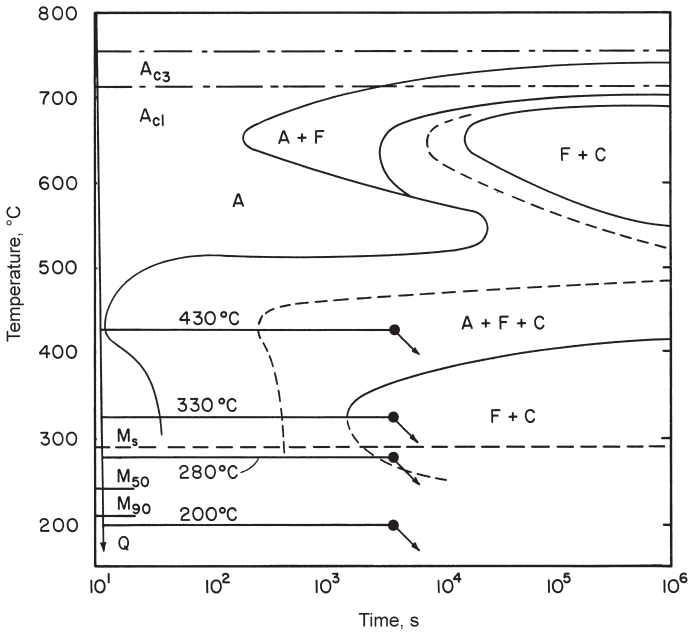

Fig. 15.37 Isothermal transformation diagram for 4340 steel and isothermal heat treatments applied to produce various microstructures for fracture evaluation. Source: Ref 15.24 as published in Ref 15.19

Mechanical Behavior of Ferrite-Carbide Bainites. Steels largely transformed to ferrite-carbide bainitic microstructures develop a wide range of strengths and ductilities. Ultimate tensile strengths of high-carbon lower bainitic microstructures may reach 1400 MPa (200 ksi), and hardness may reach 55 HRC or higher. The strengths are derived from relatively fine ferrite crystal structures, high dislocation densities within the ferritic crystals, and fine dispersions of cementite. The lower the temperature of bainite formation, the finer the carbide dispersions, and the higher the hardness and strength. Lower bainite microstructures compete well with low-temperature tempered martensites in strength and fracture resistance. Often, low-alloy steels are subjected to isothermal holds to form bainite, instead of quenching to martensite, in order to reduce the stresses that produce quench cracking. In addition, bainitic steels do not incur the additional expense of tempering.

The type of bainite affects fracture characteristics. Specimens with upper bainitic microstructures have low toughness and ductility compared with specimens with lower bainitic microstructures, and upper bainites have higher ductile-to-brittle transition temperatures. These observations were confirmed in a study of 4340 steel isothermally transformed at various temperatures, as shown in Fig. 15.37. Specimens quenched in oil and tempered at 200 °C (390 °F) had tempered martensite microstructures

with hardness of 52 HRC; those held at 200 °C (390 °F) also transformed to tempered martensite with hardness 52 HRC; those held at 280 and 330 °C (540 and 630 °F) transformed largely to lower bainite with hardness of 50 and 44 HRC, respectively; and those transformed at 430 °C (810 °F) transformed largely to upper bainite with hardness of 32 HRC.

The results of room-temperature instrumented Charpy V-notch testing of the 4340 specimens are shown in Fig. 15.38. Instrumented impact testing measures both initiation and propagation energies. The fracture energy of the specimens with the upper bainitic microstructures was significantly lower than those with tempered martensite or lower bainite. When fracture was initiated in the upper bainite, the propagation energy dropped to zero. Fractography of the upper bainitic specimens showed, except at initiation at the notch root, that the fracture surface consisted entirely of cleavage fracture (Fig. 15.39b), a result attributed to the coarse interlath carbides and common cleavage plane of the parallel ferrite crystal in packets of upper bainite. In contrast, the fracture surfaces of the specimens transformed to tempered martensite consisted of ductile microvoid coalescence (Fig. 15.39a). Although microstructures with lower strength and hardness typically show better ductility and fracture resistance than microstructures with higher hardness, the behavior of upper bainite, with its lower hardness compared with other microstructures in 4340 steel, contradicts this general rule. A study of the fracture behavior of 4150 steel isothermally transformed to lower and upper bainite confirms the strong susceptibility of upper bainite to cleavage fracture despite its lower hardness and strength relative to lower bainitic microstructures.

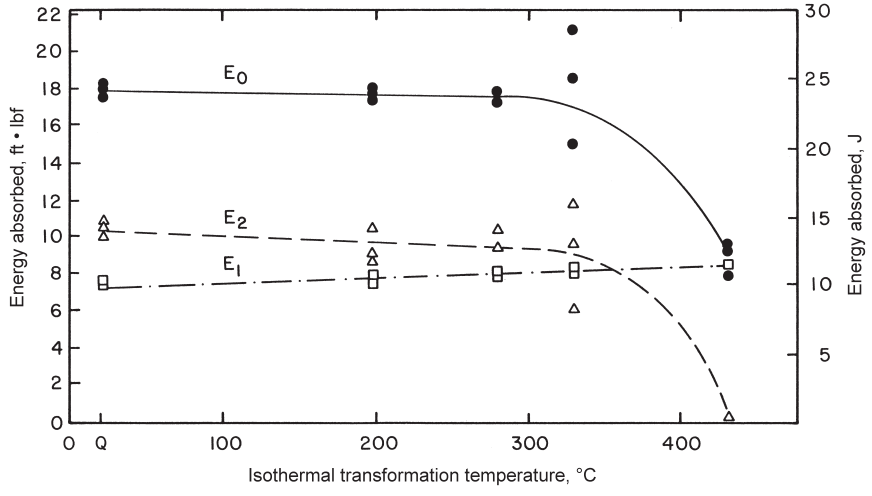

Fig. 15.38 Impact energy absorbed as a function of isothermal transformation temperature for specimens of 4340 steel. E_0, total energy absorbed; E_1, fracture initiation energy; E_2, fracture propagation energy. Source: Ref 15.24 as published in Ref 15.19

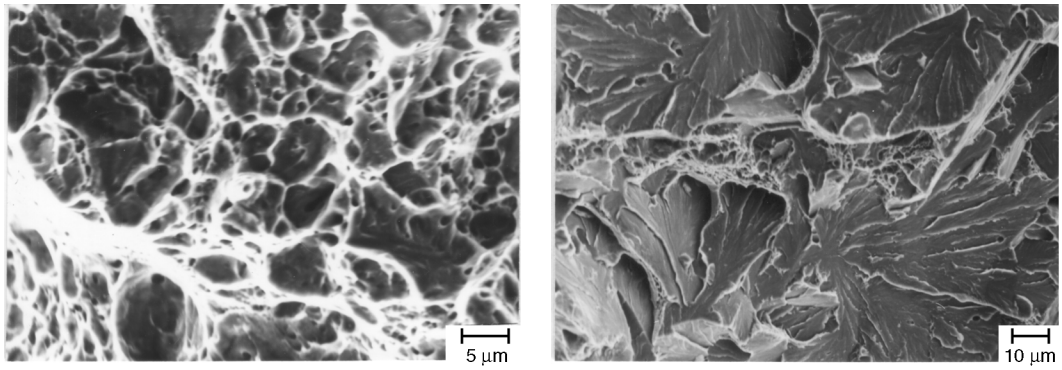

Fig. 15.39 Fracture morphologies of fracture surfaces of 4340 steel Charpy V-notch specimens heat treated as: (a) oil quenched and tempered at 200 °C (390 °F), and (b) isothermally transformed at 430 °C (810 °F). Source: Ref 15.24 as published in Ref 15.19

ACKNOWLEDGMENTS

The contents of this chapter came from *Elements of Metallurgy and Engineering Alloys* by F.C. Campbell, ASM International, 2008; "Martensitic Structures," in *Metallography and Microstructures,* Vol 9, *ASM Handbook*, ASM International, 2004; "Ferrous Martensite," by R.M. Deacon in *Metallography and Microstructures,* Vol 9, *ASM Handbook*, ASM International, 2004; "Nonferrous Martensite," by F.C. Gift, Jr. in *Metallography and Microstructures,* Vol 9, *ASM Handbook*, ASM International, 2004; and "Bainite: An Intermediate Temperature Transformation Product of Austenite," by G. Krauss in *Steels: Processing, Structure, and Performance*, ASM International, 2005.

REFERENCES

15.1 W.F. Smith, *Principles of Materials Science and Engineering*, McGraw-Hill, 1986

15.2 F.C. Campbell, *Elements of Metallurgy and Engineering Alloys*, ASM International, 2008

15.3 Martensitic Structures, *Metallography and Microstructures,* Vol 9, *ASM Handbook*, ASM International, 2004, p 165–178

15.4 B.L. Bramfitt, Effects of Composition, Processing, and Structure on Properties of Irons and Steels, *Materials Selection and Design*, Vol 20, *ASM Handbook,* ASM International, 1997

15.5 G. Krauss, Microstructures, Processing, and Properties of Steels, *Properties and Selections: Irons, Steels, and High-Performance Alloys*, Vol 1, *ASM Handbook,* ASM International, 1990

15.6 D. Aliya and S. Lampman, Physical Metallurgy Concepts in Interpretation of Microstructures, *Metallography and Microstructures*, Vol 9, *ASM Handbook,* ASM International, 2004

15.7 A.K. Sinha, *Ferrous Physical Metallurgy,* Butterworth Publishers, 1989
15.8 G. Krauss, *Principles of Heat Treatment of Steel,* American Society for Metals, 1985
15.9 R.M. Deacon, Ferrous Martensite, *Metallography and Microstructures,* Vol 9, *ASM Handbook*, ASM International, 2004, p 165–170
15.10 A.R. Marder, Structure-Property Relationships in Ferrous Transformation Products, *Phase Transformation of Ferrous Alloys,* TMS, 1984, p 11–41
15.11 B.A. Lindsley and A.R. Marder, The Morphology and Coarsening Kinetics of Spheroidized Fe-C Binary Alloys, *Acta Mater.,* Vol 46, 1997, p 341–351
15.12 H. Scherngell and A.C. Kneissl, *Acta Mater.,* Vol 50, 2002, p 328
15.13 F.C. Gift, Jr., Nonferrous Martensite, *Metallography and Microstructures,* Vol 9, *ASM Handbook*, ASM International, 2004, p 172–175
15.14 J. Dutkiewicz, T. Czeppe, and J. Morgiel, *Mater. Sci. Eng.,* Vol A273–275, 1999, p 706
15.15 D. Schryvers and D. Holland-Moritz, *Mater. Sci. Eng.,* Vol A273–275, 1999, p 699
15.16 D.E. Hodgson, M.H. Wu, and R.J. Biermann, Shape Memory Alloys, *Properties and Selection: Nonferrous Alloys and Special-Purpose Materials*, Vol 2, *ASM Handbook,* ASM International, 1990
15.17 C. Zener, Kinetics of the Decomposition of Austenite, *Transactions AIME,* Vol 167, 1946, p 550–595
15.18 H.K.D.H. Bhadeshia, *Bainite in Steels,* Book No. 504, The Institute of Materials, London, 1992
15.19 G. Krauss, Chapter 6: Bainite: An Intermediate Temperature Transformation Product of Austenite, *Steels: Processing, Structure, and Performance*, ASM International, 2005
15.20 H.I. Aaronson, W.T. Reynolds, Jr., G.J. Shiflet, and G. Spanos, Bainite Viewed Three Different Ways, *Metall. Trans. A,* Vol 21A, 1990, p 1343–1380
15.21 R.F. Hehemann and A.R. Troiano, The Bainite Transformation, *Met. Prog.,* 1956, Vol 70 (No. 2), p 97–104
15.22 F.B. Pickering, The Structure and Properties of Bainite in Steels, *Transformation and Hardenability in Steels,* Climax Molybdenum Company of Michigan, Ann Arbor, MI, 1977, p 109–132
15.23 R.F. Hehemann, Ferrous and Nonferrous Bainitic Structures, *Metallography, Structures and Phase Diagrams,* Vol 8, *Metals Handbook,* 8th ed., American Society for Metals, 1973, p 194–196
15.24 G. Baozhu and G. Krauss, The Effect of Low-Temperature Isothermal Heat Treatments on the Fracture of 4340 Steel, *J. Heat Treating,* Vol 4 (No. 4), 1986, p 365–372